[34] Ylinen LM, Price AJ, Rasaiyaah J, Hué S, Rose NJ, Marzetta F, et al. Conformational adaptation of Asian macaque TRIMCyp directs lineage specific antiviral activity. PLoS Pathog 2010;6:e1001062.
[35] Wu F, Kirmaier A, Goeken R, Ourmanov I, Hall L, Morgan JS, et al. TRIM5 alpha drives SIVsmm evolution in rhesus macaques. PLoS Pathog 2013;9:e1003577.
[36] Doi N, Fujiwara S, Adachi A, Nomaguchi M. Rhesus M1.3S cells suitable for biological evaluation of macaque-tropic HIV/SIV clones. Front Microbiol 2011;2:115.
[37] von Schwedler UK, Stray KM, Garrus JE, Sundquist WI. Functional surfaces of the human immunodeficiency virus type 1 capsid protein. J Virol 2003;77:5439–50.
[38] Nomaguchi M, Doi N, Fujiwara S, Saito A, Akari H, Nakayama EE, et al. Systemic biological analysis of the mutations in two distinct HIV-1mt genomes occurred during replication in macaque cells. Microbes Infect 2013;15:319–28.

JVI
Journals.ASM.org

Generation of Rhesus Macaque-Tropic HIV-1 Clones That Are Resistant to Major Anti-HIV-1 Restriction Factors

Masako Nomaguchi,[a] Masaru Yokoyama,[b] Ken Kono,[c] Emi E. Nakayama,[c] Tatsuo Shioda,[c] Naoya Doi,[a,d] Sachi Fujiwara,[a] Akatsuki Saito,[d,e] Hirofumi Akari,[e] Kei Miyakawa,[d,f] Akihide Ryo,[f] Hirotaka Ode,[d,g] Yasumasa Iwatani,[g] Tomoyuki Miura,[h] Tatsuhiko Igarashi,[h] Hironori Sato,[b] Akio Adachi[a]

Department of Microbiology, Institute of Health Biosciences, The University of Tokushima Graduate School, Tokushima, Tokushima, Japan[a]; Laboratory of Viral Genomics, Pathogen Genomics Center, National Institute of Infectious Diseases, Musashimurayama, Tokyo, Japan[b]; Department of Viral Infections, Research Institute for Microbial Diseases, Osaka University, Suita, Osaka, Japan[c]; Japanese Foundation for AIDS Prevention, Chiyoda-ku, Tokyo, Japan[d]; Section of Comparative Immunology and Microbiology, Center for Human Evolution Modeling Research, Primate Research Institute, Kyoto University, Inuyama, Aichi, Japan[e]; Department of Microbiology, Yokohama City University School of Medicine, Yokohama, Kanagawa, Japan[f]; Clinical Research Center, Department of Infectious Diseases and Immunology, National Hospital Organization Nagoya Medical Center, Nagoya, Aichi, Japan[g]; Laboratory of Primate Model, Experimental Research Center for Infectious Diseases, Institute for Virus Research, Kyoto University, Kyoto, Kyoto, Japan[h]

Human immunodeficiency virus type 1 (HIV-1) replication in macaque cells is restricted mainly by antiviral cellular APOBEC3, TRIM5α/TRIM5CypA, and tetherin proteins. For basic and clinical HIV-1/AIDS studies, efforts to construct macaque-tropic HIV-1 (HIV-1mt) have been made by us and others. Although rhesus macaques are commonly and successfully used as infection models, no HIV-1 derivatives suitable for *in vivo* rhesus research are available to date. In this study, to obtain novel HIV-1mt clones that are resistant to major restriction factors, we altered Gag and Vpu of our best HIV-1mt clone described previously. First, by sequence- and structure-guided mutagenesis, three amino acid residues in Gag-capsid (CA) (M94L/R98S/G114Q) were found to be responsible for viral growth enhancement in a macaque cell line. Results of *in vitro* TRIM5α susceptibility testing of HIV-1mt carrying these substitutions correlated well with the increased viral replication potential in macaque peripheral blood mononuclear cells (PBMCs) with different *TRIM5* alleles, suggesting that the three amino acids in HIV-1mt CA are involved in the interaction with TRIM5α. Second, we replaced the transmembrane domain of Vpu of this clone with the corresponding region of simian immunodeficiency virus SIVgsn166 Vpu. The resultant clone, MN4/LSDQgtu, was able to antagonize macaque but not human tetherin, and its Vpu effectively functioned during viral replication in a macaque cell line. Notably, MN4/LSDQgtu grew comparably to SIVmac239 and much better than any of our other HIV-1mt clones in rhesus macaque PBMCs. In sum, MN4/LSDQgtu is the first HIV-1 derivative that exhibits resistance to the major restriction factors in rhesus macaque cells.

Human immunodeficiency virus type 1 (HIV-1) has spread globally in human populations following cross-species transmission of simian immunodeficiency virus (SIV) from chimpanzees (1, 2). HIV-1 replicates well in humans and causes disease-inducing persistent infection only in humans. HIV-1 infection is impeded after virus entry in rhesus macaques (RhMs) and cynomolgus macaques (CyMs), which are frequently used for experimental viral infection studies (3). The block of HIV-1 infection in macaque cells is attributable to intrinsic restriction factors, including APOBEC3, TRIM5α/TRIM5CypA, and tetherin proteins (1, 4–6). These factors exert their antiretroviral activity in a species-specific manner, and HIV-1 effectively subverts their counterparts in human cells (1, 4–6). In contrast, a standard pathogenic clone, SIVmac239, for AIDS model studies evades the restriction factors and replicates well in macaques. HIV-1 and SIVmac239 are mutually related primate lentiviruses and cause AIDS in their respective hosts. Nevertheless, there are significant differences between the two viruses in genome organization, the viral replication profile *in vivo*, and disease progression (7–9). It is therefore most preferable to generate pathogenic HIV-1 derivatives to establish AIDS macaque models (7–9). Importantly, construction of HIV-1 derivatives that overcome the species barrier would contribute much to the understanding of the molecular interaction of viral and host proteins.

Of the intrinsic restriction factors in macaque cells, major determinants of the HIV-1 host range are the APOBEC3 and TRIM5 proteins (4, 8, 10). APOBEC3G is the strongest inhibitor of HIV-1 replication among APOBEC3 family proteins. It exhibits cytidine deaminase activity and causes hypermutation in the HIV-1 genome following incorporation into progeny virions in producer cells. HIV-1 Vif is able to degrade human APOBEC3G and neutralize its antiviral activity but is not effective against macaque APOBEC3G (4–6, 11, 12). Macaque TRIM5 proteins recognize and interact with the incoming HIV-1 cores and inhibit viral infection prior to reverse transcription (4, 6, 13, 14). TRIM5 proteins are composed of N-terminal RING, B-box 2, and coiled-coil domains. The C termini of TRIM5α and TRIM5CypA are the B30.2/SPRY and cyclophilin A (CypA) domains, respectively. All these domains in TRIM5 proteins are necessary to exert full restriction activity. Although the mechanism underlying TRIM5-mediated restriction has not been completely defined, inhibition of viral infection is initiated by capsid (CA) recognition with the

Received 7 June 2013 Accepted 9 August 2013
Published ahead of print 21 August 2013
Address correspondence to Hironori Sato, hirosato@nih.go.jp, or Akio Adachi, adachi@basic.med.tokushima-u.ac.jp.
M.N. and M.Y. contributed equally to this article.

doi:10.1128/JVI.01549-13

B30.2/SPRY or CypA domain. Sequence variation in the two domains determines species-specific restriction of retroviral infection. RhM *TRIM5* genes have been reported to be highly polymorphic (4, 6, 13, 14). Tetherin works as a virion release inhibition factor, and HIV-1 Vpu counteracts human but not macaque tetherin (4–6, 15). Tetherin may not be a potent barrier to limit cross-species transmission relative to APOBEC3G and TRIM5 proteins. However, tetherin antagonism is important for viral replication *in vivo*, because most primate lentiviruses have the ability to counteract tetherin, and tetherin-mediated restriction contributes to inhibiting viral replication *in vivo* (4, 5, 15). Recently, a novel anti-HIV-1 factor, SAMHD1, has been identified (4–6). Several Vpx and Vpr proteins appear to degrade SAMHD1 in a species-specific manner. However, SAMHD1 may be a weak species barrier, since HIV-1 has spread successfully and continuously in humans despite the lack of anti-SAMHD1 activity (4).

We and others have reported the construction of HIV-1 derivatives that have the ability to evade restriction factors for macaque model studies (16–21). As a common feature, all reported macaque-tropic HIV-1 (HIV-1mt) clones have the *vif* gene, which can neutralize macaque APOBEC3G (e.g., SIVmac239 *vif*). This modification is essential to evade APOBEC3G restriction and to gain the ability to replicate in macaque cells. To circumvent the restriction by TRIM5 proteins, two approaches have been taken. One approach is the use of pig-tailed macaques that do not express HIV-1-restrictive TRIM5 proteins. In this case, HIV-1 derivatives carrying authentic HIV-1 CA have been used as challenge viruses (stHIV-1_{SV} [16] and HSIV-vif [21]). Another approach is the replacement of the entire HIV-1 CA with the corresponding region of SIVmac239 (stHIV-1_{SCA+SV} [16, 17]). Although stHIV-1_{SCA+SV} replicates well in RhM cells, the CA region is not derived from HIV-1. Recently, chimeric viruses between simian-human immunodeficiency virus ($SHIV_{DH12}$ and $SHIV_{AD8}$) and an HIV-1 derivative (stHIV-1gsnU) that display anti-macaque tetherin activity have been reported (22, 23). However, the former construct is SHIV, and the latter is pig-tailed macaque-tropic HIV-1 carrying full-length SIVgsn71 (SIV from greater spot-nosed monkey) Vpu. While RhMs have been commonly and frequently used for viral infection experiments, no RhM-tropic HIV-1 derivatives that exhibit resistance to known major intrinsic restriction factors (APOBEC3, TRIM5, and tetherin proteins) have been reported.

We have previously described a unique HIV-1mt clone, designated MN4Rh-3, which can evade APOBEC3 and TRIM5CypA proteins but not TRIM5α and tetherin restrictions in macaque cells (Fig. 1) (19, 24). In this study, we generated new HIV-1mt clones from MN4Rh-3 that potentially possess an improved capacity to antagonize RhM TRIM5α and tetherin proteins. First, we constructed a number of MN4Rh-3 CA mutant clones; examined their growth potentials in an RhM lymphocyte cell line, M1.3S (25); and selected a new HIV-1mt clone, MN4/LSDQ, carrying only three amino acid substitutions in MN4Rh-3 CA (Fig. 1). MN4/LSDQ exhibited enhanced growth potential accompanied by increased resistance to macaque TRIM5α restriction. Next, we replaced the transmembrane (TM) domain of MN4/LSDQ Vpu with the corresponding region of SIVgsn166 (another SIVgsn) Vpu, which shows anti-macaque tetherin activity (26). The resultant clone, MN4/LSDQgtu, gained the ability to antagonize specifically macaque tetherin (Fig. 1). The replication efficiency of MN4/LSDQgtu in RhM peripheral blood mononuclear cells (PBMCs) was comparable to that of SIVmac239 and was superior to those of the other HIV-1mt clones (MN4Rh-3 and MN4/LSDQ). MN4/LSDQgtu is the first HIV-1 derivative that is highly resistant to the known major restriction factors (APOBEC3, TRIM5, and tetherin proteins) in RhM cells. Generation of MN4/LSDQgtu also served to find amino acid residues in CA involved in the interaction with macaque TRIM5α and to verify HIV-1mt growth enhancement in macaque cells by macaque tetherin antagonism.

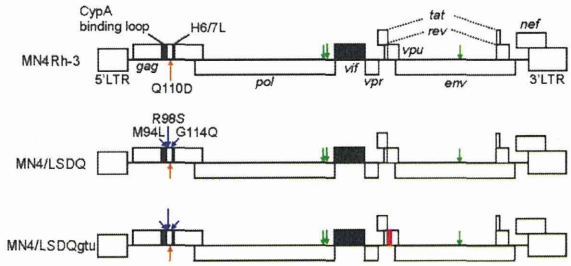

FIG 1 Proviral genome structures of various HIV-1mt clones. HIV-1 NL4-3 (32), SIVmac239 MA239 (71), and SIVgsn166 (GenBank accession number AF468659) sequences are indicated by white, black, and red areas, respectively. Green arrows show adaptive mutations that enhance viral growth potential (47). Orange arrows show the CA-Q110D mutation that augments viral growth in macaque cells/monkeys (19, 24). Blue arrows indicate CA substitutions (M94L/R98S/G114Q) identified in this study that are responsible for viral growth enhancement. H6/7L, loop between helices 6 and 7 in Gag-CA.

MATERIALS AND METHODS

Cells. An RhM lymphocyte cell line, M1.3S (25), was maintained in RPMI 1640 medium containing 10% heat-inactivated fetal bovine serum (FBS) and 50 units/ml of recombinant human interleukin-2 (IL-2) (Bio-Rad Laboratories Inc., Hercules, CA). The human monolayer cell lines 293T (27) and HEp2 (ATCC CCL-23) and the RhM kidney cell line LLC-MK2 (ATCC CCL-7) were maintained in Eagle's minimal essential medium (MEM) containing 10% FBS. MAGI cells (28) were cultured in MEM containing 10% FBS, 200 μg/ml G418 (Sigma-Aldrich Co., St. Louis, MO), and 100 μg/ml hygromycin B (Sigma-Aldrich Co.).

Plasmid DNA. The construction of MN4Rh-3, SIVmac239 clone MA239N, and its *nef*-deficient variant MA239N-ΔN was described previously (19, 25). CA alterations of HIV-1mt proviral clones were performed by replacing target sites of HIV-1mt CA with the corresponding sites of SIVmac239 (both codons and amino acids were changed to those of SIVmac239) by using the QuikChange site-directed mutagenesis kit (Agilent Technologies Inc., Santa Clara, CA). MN4/LSDQ was generated by introducing the following codon/amino acid substitutions into MN4Rh-3 (uppercase letters represent amino acids and lowercase letters represent codons): M(atg) to L(ctt) at amino acid position 94, R(agg) to S(tca) at position 98, and G(gga) to Q(cag) at position 114. Each *vpu* gene of SIVmon (SIV from mona monkey)/SIVmus (SIV from mustached monkey)/SIVgsn (SIVmon/mus/gsn) was synthesized (TaKaRa Bio Inc., Otsu, Japan) and cloned into pSG-cFLAG to express mon-, mus-, and gsn-Vpu, respectively, as described previously (29). Full-length Vpu sequences composed of the TM domain of SIVmon/mus/gsn Vpu and the cytoplasmic domain of HIV-1_{NL4-3} Vpu (monTM-, musTM-, and gsnTM-Vpu, respectively) were made by overlapping PCR and inserted into the pSG-cFLAG expression vector, as described previously (29). The resultant clones were designated pSG-VpucFLAG constructs. RhM and human tetherin sequences were amplified by PCR using cDNAs from M1.3S cells and HeLa cells, respectively. The amplified products were cloned into the pCIneo vector (Promega Corporation, Madison, WI) to generate pCIneo-RhM tetherin and pCIneo-Human tetherin. The sequence of RhM tetherin from M1.3S cells was identical to that of an RhM

tetherin variant [Mac(m)3] (30, 31). For flow cytometry analysis, pIRES-HIV-1-Vpu-hrGFP and pIRES-gsnTM-Vpu-hrGFP were constructed as described previously (29). The MN4/LSDQdtu clone was constructed by replacing the TM domain of MN4/LSDQ Vpu with the corresponding region of HIV-1_{DH12} Vpu (22) by using the QuikChange site-directed mutagenesis kit (Agilent Technologies Inc.). The MN4/LSDQgtu clone was generated by overlapping PCR between MN4/LSDQ and gsnTM-Vpu. *vpu*-deficient HIV-1mt clones were constructed by changing the initiation codon (ATG) to AGG and the second codon of each construct to TAG (stop codon).

Virus stocks and reverse transcriptase assay. Virus stocks were prepared from 293T cells transfected with proviral clones by the calcium-phosphate coprecipitation method (32). Virion-associated reverse transcriptase (RT) activity was measured as described previously (33), with the following modifications: 5 μl of culture supernatant was mixed with 25 μl of an RT reaction mixture containing a template primer of poly(A) (500 μg/ml; Midland Certified Reagent Company Inc., Midland, TX) and oligo$(dT)_{12–18}$ (1.25 μg/ml; New England BioLabs Inc., Ipswich, MA) in 50 mM Tris (pH 7.8), 75 mM KCl, 2 mM dithiothreitol, 5 mM $MgCl_2$, 0.05% Nonidet P-40, and 9.25 kBq of [α-^{32}P]dTTP (29.6 TBq/mmol; Perkin-Elmer Inc., Waltham, MA). After incubation at 37°C for 3 h, 10 μl of the reaction mixture was spotted onto DE81 anion-exchange paper (GE Healthcare UK Ltd., Buckinghamshire, England) and washed four times with 2× SSC (0.3 M NaCl plus 0.03 M sodium citrate) to remove unincorporated [α-^{32}P]dTTP. Spots were then counted with a scintillation counter.

Virus replication assays. Virus replication in M1.3S cells was monitored as described previously (25). For infection of macaque primary cells, RhM and CyM PBMCs were separated by Ficoll-Paque Plus (GE Healthcare UK Ltd.) and stimulated with RPMI 1640 medium containing 10% FBS, 50 units/ml of recombinant human IL-2, and 2 μg/ml of phytohemagglutinin L (PHA-L) (Roche Diagnostics GmbH, Mannheim, Germany). Primary PBMCs without $CD8^+$ cell depletion were used in this study. On day 3 poststimulation, cells were spin infected (34) with equal amounts of viruses prepared from transfected 293T cells and cultured in the presence of IL-2. Viral growth was monitored by RT activity released into the culture supernatants. The genotype of *TRIM5* alleles was analyzed as described previously (35).

TRIM5α susceptibility assays. Assays using recombinant Sendai virus (SeV)-RhM TRIM5α and SeV-CyM TRIM5α expression systems were performed as described previously (36). MT4 cells (10^5) were infected with SeV expressing each TRIM5α at a multiplicity of infection of 10 PFU per cell and incubated at 37°C for 9 h. Cells were then superinfected with HIV-1mt derivatives (20 ng of Gag-p24) or SIVmac239 (20 ng of Gag-p27). Culture supernatants were collected at intervals, and the amount of Gag-p24 or Gag-p27 produced was determined by using RETROtek antigen enzyme-linked immunosorbent assay (ELISA) kits (ZeptoMetrix Corporation, Buffalo, NY).

Virion release assays. Tetherin-null 293T cells were used for virion release assays. For analysis of Vpu expression vectors, subconfluent 293T cells in 24-well dishes were cotransfected with *vpu*-deficient MN4Rh-3 (300 ng), pCIneo-RhM tetherin (5 ng), and various pSG-VpucFLAG vectors (200 ng) by using Lipofectamine 2000 (Life Technologies Corporation, Carlsbad, CA). On day 2 posttransfection, virion production in the cell culture supernatants was measured by RT assays. For analysis of proviral clones, 700 ng of MA239N/MA239N-ΔN or 300 ng of MN4 derivatives and an appropriate amount of pCIneo-RhM tetherin or pCIneo-Human tetherin were used for cotransfection.

Flow cytometry analysis. Flow cytometry analysis was performed to examine cell surface CD4 or tetherin downregulation by Vpu, as described previously (29). For analysis of cell surface CD4, MAGI cells in 60-mm dishes were transfected with pIRES-hrGFP-Vpu vectors. On day 2 posttransfection, cells were trypsinized, washed with phosphate-buffered saline (PBS), and resuspended in PBS containing 10% FBS. Cells were then stained with a phycoerythrin (PE)-conjugated mouse anti-human CD4 antibody (BD Biosciences, San Jose, CA). For analysis of cell surface tetherin, LLC-MK2 or HEp2 cells in 60-mm dishes were transfected with pIRES-hrGFP-Vpu vectors and harvested as described above. Cells were then reacted with an anti-HM1.24 monoclonal antibody (a generous gift from Chugai Pharmaceutical Co. Ltd., Chuo-ku, Japan) and stained with a secondary PE-conjugated anti-mouse Ig antibody (BD Biosciences). Stained cells were analyzed with a FACSCalibur instrument using CELLQuest software (BD Biosciences).

Prediction of the effects of amino acid substitutions on the stability of the HIV-1mt CA N-terminal domain. The three-dimensional (3-D) model of the HIV-1mt CA N-terminal domain (NTD) was constructed by homology modeling using "MOE-Align" and "MOE-Homology" in the Molecular Operating Environment (MOE) (Chemical Computing Group Inc., Quebec, Canada) and refined as described previously (19). The crystal structure of the HIV-1 CA NTD at a resolution of 2.00 Å (Protein Data Bank [PDB] accession number 1M9C) (37) was used as the modeling template. The changes in the stability of the CA NTD by mutations were computed by using the Protein Design application in MOE. Single-point mutations on the CA protein were generated, and ensembles of protein conformations were generated by using the LowMode MD module in MOE to calculate average stability using Boltzmann distribution. Finally, the stability scores of the structures refined by energy minimization were obtained through the stability scoring function of the Protein Design application.

Structural modeling of the Vpu TM domains. We first constructed 3-D structural models for monomers of Vpu TM domains encoded in three HIV-1mt clones (MN4/LSDQ, MN4/LSDQdtu, and MN4/LSDQgtu) with PyMOL on the basis of the previously reported structure of the HIV-1_{BH10} Vpu TM domain (PDB accession number 1PI8) (38). The HIV-1_{BH10} Vpu TM domain has a sequence identical to that of the MN4/LSDQ Vpu TM domain. The 3-D structures of their tetramers were then predicted from the constructed monomer structures with Rosetta 3.4 (39). We performed symmetry docking and predicted 10,000 tetramer structures for each molecule. Among the predicted structures, the structure with the best total score was selected as the model of the respective molecules. We compared the predicted tetramer structure of the MN4/LSDQ Vpu TM domain with the nuclear magnetic resonance (NMR) structure of the tetramer of the HIV-1_{BH10} Vpu TM domain (PDB accession number 1PI8). Their overall structures were highly similar. The root mean square deviation of C-α atoms between them was 1.64 Å.

RESULTS

Sequence homology- and structure-based modifications led to the identification of HIV-1mt CA residues that are responsible for the enhancement of viral growth in RhM cells. TRIM5 proteins inhibit retroviral infection in a species-specific manner. The RhM *TRIM5* coding sequence is highly polymorphic, and common RhM *TRIM5* alleles (*Mamu-1* to *Mamu-7*) can be divided into three groups based on polymorphisms at amino acid positions 339 to 341 within the B30.2/SPRY domain: $TRIM5^{TFP}$ (*Mamu-1* to *Mamu-3*), $TRIM5^{Q}$ (*Mamu-4* to *Mamu-6*), and $TRIM5^{CypA}$ (*Mamu-7*) (35, 40, 41). CyM TRIM5α has a Q residue at the corresponding site ($TRIM5^{Q}$), and CyM TRIM5CypA has a CypA sequence slightly different from that of RhM TRIM5CypA (42, 43). RhM and CyM TRIM5α proteins encoded by $TRIM5^{TFP}$ and $TRIM5^{Q}$ inhibit HIV-1 infection. On the other hand, CyM TRIM5CypA, but not RhM TRIM5CypA, restricts HIV-1 replication (42, 43). We have shown previously that a CXCR4-tropic MN4Rh-3 clone evaded CyM TRIM5CypA but was susceptible to TRIM5α restriction (19) and that its replication in *TRIM5*α homozygous CyM PBMCs/individuals was strongly restricted (24). Similarly, MN4Rh-3 replicated quite well in a CyM HSC-F cell line ($TRIM5^{Q/CypA}$) but very poorly in an RhM M1.3S cell line

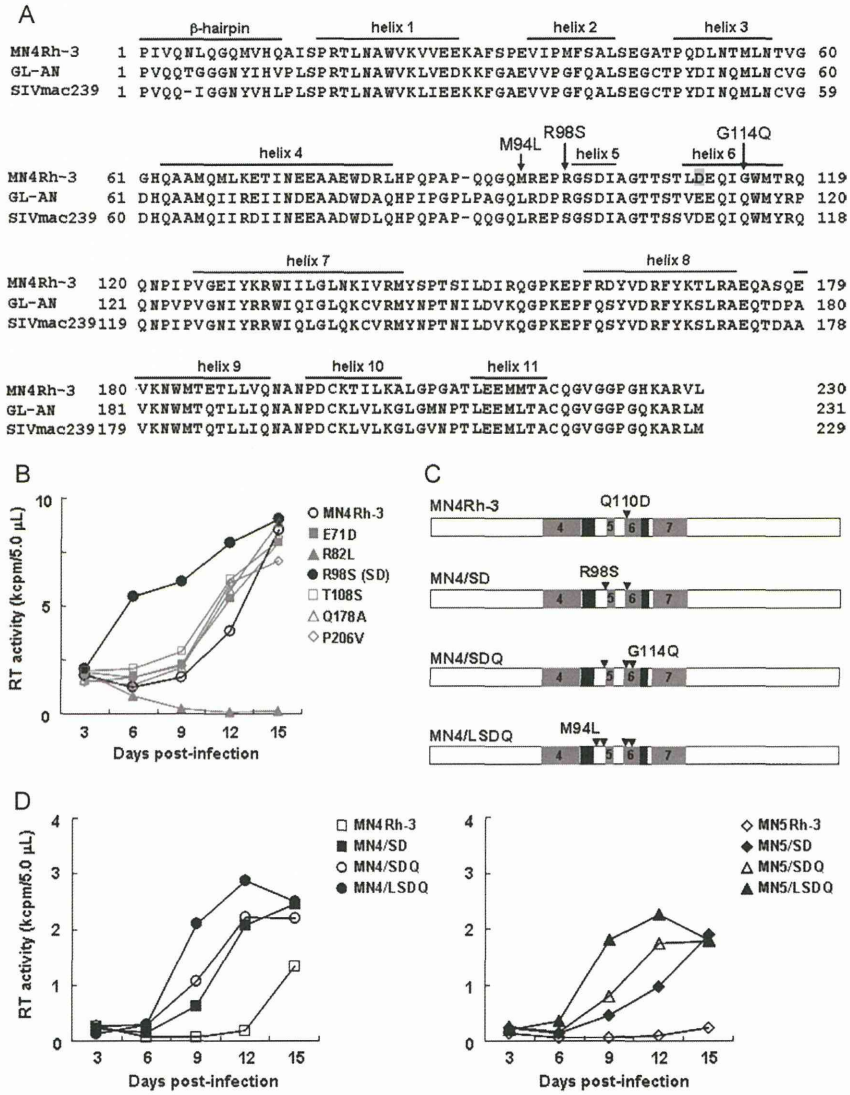

FIG 2 Identification of amino acid residues in HIV-1mt CA that are critical for viral growth enhancement in macaque cells. (A) Alignment of Gag-CA sequences. CA amino acid sequences of HIV-1mt MN4Rh-3 (19, 24), HIV-2 GL-AN (72), and SIVmac239 MA239 (71) are aligned. The N-terminal β-hairpin and helices 1 to 11 are indicated based on previously reported analyses (50, 73). The CA-Q110D mutation in MN4Rh-3 (19, 24) is shaded. Substitutions of three amino acids that contribute to the enhancement of HIV-1mt growth in macaque cells, described in this work, are indicated by arrows. (B) Growth kinetics of a parental clone, MN4Rh-3, and its CA mutants carrying a single-amino-acid change (see Table 1 for the mutants). Viruses were prepared from 293T cells transfected with the proviral clones indicated, and equal amounts (2×10^6 RT units) were inoculated into M1.3S cells (3×10^5 cells). Virus replication was monitored by RT activity released into the culture supernatants. Representative data from two independent experiments are shown. (C) Schematic CA structure of HIV-1mt clones. Amino acid substitutions are indicated in the order in which they were introduced into HIV-1mt CA. Black areas show sequences from SIVmac239. Helices 4 to 7 are shown as gray areas with the helix number. (D) Growth kinetics of CXCR4-tropic (left) and CCR5-tropic (right) HIV-1mt clones with different CA proteins (see reference 19 for CCR5-tropic MN5Rh-3). Viruses were prepared from 293T cells transfected with the indicated proviral clones, and equal amounts (2.5×10^6 RT units) were inoculated into M1.3S cells (10^6 cells). Virus replication was monitored by RT activity released into the culture supernatants. Representative data from two independent experiments are shown.

(*TRIM5*$^{TFP/TFP}$) (data not shown). Besides being a TRIM5α target, Gag-CA functions in various viral replication steps (44, 45). We thus used the M1.3S cell line as a target for multicycle infection to screen viral clones with increased replication potential following CA mutagenesis.

Modifications of MN4Rh-3 CA were performed based on sequence homology and structural modeling. As shown in Fig. 2A, the amino acid sequence identity of CA between HIV-1 and SIVmac239 is not high (~67% for SIVmac239 versus HIV-1_{NL4-3} and ~72% for SIVmac239 versus MN4Rh-3), but sequences are

relatively well conserved between HIV-2 and SIVmac239 (~90% for SIVmac239 versus HIV-2_{GL-AN}). Nevertheless, macaque TRIM5α restricts HIV-1 and HIV-2 infection but not SIVmac239. This distinct susceptibility to macaque TRIM5α results from the different CA sequences of each virus. We first selected amino acid residues in MN4Rh-3/HIV-2_{GL-AN} CA that are different from those of SIVmac239 CA and replaced these target residues with those of SIVmac239 (Table 1, MN4/SD and initial screening). The resultant clones were examined for their growth potential in M1.3S cells (Fig. 2B and Table 1). Of 25 clones tested, only MN4Rh-3 carrying an R98S change in CA (MN4/SD) exhibited enhanced viral growth efficiency (Table 1 and Fig. 2B). We previously found a growth-enhancing mutation, G114E, in CA by HIV-1mt adaptation in macaque cells (19). Since viral replication efficiency was decreased by the introduction of G114E into MN4Rh-3 (data not shown), we introduced an SIVmac239 CA-type G114Q mutation into the MN4/SD clone, and the resultant clone was designated MN4/SDQ (Fig. 2C and D). Moreover, we predicted an additional mutation that might improve the growth ability of MN4Rh-3 in macaque cells. Using HIV-2 CA, we previously found a key role of hydrogen bond formation between D97 within H4/5L (a loop between helices 4 and 5) and R119 within H6/7L (a loop between helices 6 and 7) in determining viral sensitivity to TRIM5α: TRIM5α-sensitive CA had a common H4/5L conformation with a decreased probability of hydrogen bond formation (46). The corresponding hydrogen bond was predicted to be formed between E96 in H4/5L and R118 in H6/7L of the MN4Rh-3 CA NTD. We assumed that the simultaneous introduction of SIV-CA-like amino acid residues at M94 in H4/5L and G114 in helix 6 might imitate the structural property of the SIVmac239 CA NTD surface for TRIM5α resistance and might be beneficial to improve the growth ability of MN4Rh-3 in macaque cells. The M94 residue is located in H4/5L, protruding its side chain near the G114 residue in helix 6. We therefore generated MN4/SDQ carrying the M94L mutation (MN4/LSDQ) (Fig. 2C and D). Three-dimensional locations of M94L, R98S, Q110D, and G114Q in the CA NTD are shown in Fig. 3. In addition, we constructed a series of CCR5-tropic viruses (MN5Rh-3, MN5/SD, MN5/SDQ, and MN5/LSDQ) (Fig. 2D), which carry the Env sequence derived from NF462 and a growth-enhancing Env S304G mutation (47). The growth potential of these viruses in M1.3S cells was analyzed. As shown in Fig. 2D, viral growth potential was enhanced with increasing amino acid substitutions in CA. MN4/LSDQ and MN5/LSDQ exhibited the highest replication potential in M1.3S cells in each group.

We constructed numerous HIV-1mt clones carrying CA mutations, including those described previously (48–50). All CA mutations and the growth potentials of the mutant viruses are summarized in Table 1. In the mutants derived from four HIV-1mt clones (MN4Rh-3, MN4/SD, MN4/SDQ, and MN4/LSDQ), most amino acid substitutions gave neutral or negative effects: CA amino acid substitutions that did not alter replication efficiency (L6I, E71D, T108S, Q178A, and P206V) or those that strikingly reduced the growth potential (e.g., Q50Y, T54Q, K70R, R82L, and L83Q; more than two consecutive mutations; and mutations in the β-hairpin domain). All listed HIV-1mt clones produced a significant amount of virions from transfected 293T cells, but none of them displayed a higher replication potential than MN4/LSDQ in M1.3S cells. In sum, M94L/R98S/G114Q substitutions in CA contributed to the growth enhancement of MN4Rh-3 in macaque cells.

Prediction of the effects of amino acid substitutions on the stability of the HIV-1 CA NTD. To investigate whether the M94L, R98S, Q110D, and G114Q mutations in MN4Rh-3 CA influenced the structural property of the protein, we analyzed the changes in stability by the mutations using the Protein Design application in MOE. The changes in stability by each of the point mutations M94L, R98S, Q110D, and G114Q were −0.41, 0.09, 0.25, and −1.70 kcal/mol, respectively (Fig. 3). The data suggested distinct effects of the single mutations at positions 94, 98, 110, and 114 on the stability of the HIV-1mt CA NTD. The Q110D mutation was predicted to destabilize the CA NTD. The R98S mutation has a similar negative effect on structure but to a much lesser extent. These mutations are considered to be more or less disadvantageous in terms of the CA structure. Nevertheless, they were critical for HIV-1mt growth enhancement in macaque cells (19) (Table 1 and Fig. 2). Therefore, these mutations must have given essential functions to CA protein in viral replication, which surpassed the structural disadvantage. On the other hand, M94L and G114Q mutations were predicted to stabilize the CA NTD. Therefore, these mutations may function as compensatory mutations that can redress structural disadvantages caused by R98S and Q110D mutations and increase growth ability in macaque cells. Our experimental data on MN4Rh-3, MN5Rh-3, and their derivatives having R98S/Q110D mutations, R98S/Q110D/G114Q mutations, and M94L/R98S/Q110D/G114Q mutations (Fig. 2) are consistent with this possibility.

Enhancement of viral replication efficiency by introduction of CA mutations (M94L/R98S/G114Q) correlates well with increased resistance to TRIM5α restriction. Some particular CA alterations (M94L/R98S/G114Q) of MN4Rh-3 markedly promoted viral replication in M1.3S cells with $TRIM5^{TFP/TFP}$ (Fig. 2D). Since TRIM5 proteins are potent restriction factors as species barriers (4, 8, 10) and can affect SIV transmission/replication *in vivo* (40, 51), it was expected that CA mutations (M94L/R98S/G114Q) would increase TRIM5α resistance as well as viral growth potential. To examine the effect of CA alterations on TRIM5α resistance, we carried out TRIM5α susceptibility assays using the recombinant SeV-TRIM5α expression system (36). TRIM5α resistance, as determined by this system, has been shown to be well reflected in the viral growth potential in macaque PBMCs/individuals due to the higher expression level of TRIM5α than that in feline CRFK cells stably expressing TRIM5α (19, 24). Four HIV-1mt clones (MN4Rh-3, MN4/SD, MN4/SDQ, and MN4/LSDQ) were assayed for their resistance to RhM-TRIM5α ($TRIM5^{TFP}$) and CyM-TRIM5α ($TRIM5^{Q}$), using SIVmac239 as a positive control. As shown in Fig. 4, the growth kinetics of SIVmac239 in cells expressing RhM- or CyM-TRIM5α or control B30.2/SPRY(−) TRIM5 were similar. Consistent with a previous analysis (19), MN4Rh-3 replication was strongly restricted in both RhM- and CyM-TRIM5α-expressing cells relative to that in control cells. Of note, TRIM5α resistance of MN4/SD, MN4/SDQ, and MN4/LSDQ quite paralleled their growth ability in M1.3S cells (see Fig. 2D for virus growth). While TRIM5α resistance of MN4/SD was increased relative to that of MN4Rh-3, MN4/SDQ exhibited higher resistance, especially to CyM-TRIM5α, than MN4/SD. MN4/LSDQ, which has the highest growth potential among the four HIV-1mt clones, showed the highest level of TRIM5α resistance, especially to RhM-TRIM5α. The HIV-1mt

TABLE 1 HIV-1mt CA mutants constructed in this study

Clone designation	CA mutation(s)[b]	Growth potential[c]
MN4Rh-3[a]	None (parental clone)	++
MN4/SD	R98S	+++
MN4/SDQ	R98S, G114Q	+++
MN4/LSDQ	M94L, R98S, G114Q	++++
Initial screening		
E71D	E71D	++
R82L	R82L	−
RL82LQ	RL82, 83LQ	−
T108S	T108S	++
Q178A	Q178A	++
P206V	P206V	++
PD	L6P	−
PDQ	L6P, G114Q	−
PYD	L6P, Q50Y	+
PYDQ	L6P, Q50Y, G114Q	+
PYQD	L6P, Q50Y, T54Q	+
PYQDQ	L6P, Q50Y, T54Q, G114Q	+
GG	LQ6, 7GG	−
GG-T117Y	LQ6, 7GG, T117Y	−
IGGN	LQGQ6-9IGGN	−
IGGN-T117Y	LQGQ6-9IGGN, T117Y	−
5IGGN	NLQGQ5-9IGGN	−
YD	Q50Y	−
YDQ	Q50Y, G114Q	−
YQD	Q50Y, T54Q	−
YQDQ	Q50Y, T54Q, G114Q	−
IIRDI	MLKET68-72IIRDI	−
TDA	ASQ176-178TDA	−
VNP	PGA206-208VNP	−
Mutants from MN4/SD		
L6I-S	L6I, R98S	++
YQ-S	Q50Y, T54Q, R98S	−
DS	E71D, R98S	+++
SS	R98S, T108S	+++
SA	R98S, Q178A	+++
SV	R98S, P206V	+++
SAV	R98S, Q178A, P206V	+++
DSAV	E71D, R98S, Q178A, P206V	+++
Mutants from MN4/SDQ or MN4/LSDQ		
L6I-LSDQ	L6I, M94L, R98S, G114Q	++++
YQ-LDQ	Q50Y, T54Q, M94L, G114Q	−
YQ-SDQ	Q50Y, T54Q, R98S, G114Q	−
YQ-LSDQ	Q50Y, T54Q, M94L, R98S, G114Q	−
K70R-LSDQ	K70R, M94L, R98S, G114Q	−
E71D-LSDQ	E71D, M94L, R98S, G114Q	+++
E79D-LSDQ	E79D, M94L, R98S, G114Q	++++
R82L-LSDQ	R82L, M94L, R98S, G114Q	−
L83Q-LSDQ	L83Q, M94L, R98S, G114Q	−
T108S-LSDQ	M94L, R98S, T108S, G114Q	++++
E79D-T108S-LSDQ	E79D, M94L, R98S, T108S, G114Q	++++
E127N-LSDQ	M94L, R98S, G114Q, E127N	+++
I134Q-LSDQ	M94L, R98S, G114Q, I134Q	−
LSDQN	M94L, R98S, G114Q, S148N	−
I152V-LSDQ	M94L, R98S, G114Q, I152V	+++
LSDQA	M94L, R98S, G114Q, Q178A	++++
IY-LSDQA	L6I, M10Y, M94L, R98S, G114Q, Q178A	++
YQ-LSDQA	Q50Y, T54Q, M94L, R98S, G114Q, Q178A	−
LSDQA-P159S	M94L, R98S, G114Q, P159S, Q178A	+++

(Continued on following page)

TABLE 1 (Continued)

Clone designation	CA mutation(s)[b]	Growth potential[c]
L6I-LSDQA	L6I, M94L, R98S, G114Q, Q178A	++++
DLSDQA	E71D, M94L, R98S, G114Q, Q178A	+++
L6I-DLSDQA	L6I, E71D, M94L, R98S, G114Q, Q178A	+++
LSDQAV	M94L, R98S, G114Q, Q178A, P206V	++++
L6I-LSDQAV	L6I, M94L, R98S, G114Q, Q178A, P206V	++++
YQ-LSDQAV	Q50Y, T54Q, M94L, R98S, G114Q, Q178A, P206V	−
DLSDQAV	E71D, M94L, R98S, G114Q, Q178A, P206V	+++
L6I-DLSDQAV	L6I, E71D, M94L, R98S, G114Q, Q178A, P206V	+++
Mutants of the β-hairpin domain		
DdN5	N5 deletion	−
DdN5-Y	N5 deletion, T117Y	−
SDdN5	N5 deletion, R98S	−
SDdN5-Y	N5 deletion, R98S, T117Y	−
DQdN5-Y	N5 deletion, G114Q, T117Y	−
SDQdN5	N5 deletion, R98S, G114Q	−
SDQdN5-Y	N5 deletion, R98S, G114Q, T117Y	−
LSDQdN5	N5 deletion, M94L, R98S, G114Q	−
LSDQdN5-Y	N5 deletion, M94L, R98S, G114Q, T117Y	−
QIG-S	NLQ5-7QIG, R98S	−
QIG-SDQ	NLQ5-7QIG, R98S, G114Q	−
QIG-LSDQ	NLQ5-7QIG, M94L, R98S, G114Q	−
GGN-S	QGQ7-9GGN, R98S	−
GGN-LSDQ	QGQ7-9GGN, M94L, R98S, G114Q	−
GGN-YQ-LSDQ	QGQ7-9GGN, Q50Y, T54Q, M94L, R98S, G114Q	−
L6I-YQ-LSDQ	L6I, Q50Y, T54Q, M94L, R98S, G114Q	−
IL-LSDQA	L6I, Q13L, M94L, R98S, G114Q, Q178A	−
IL-Y-LSDQA	L6I, Q13L, M94L, R98S, G114Q, T117Y, Q178A	−
IN-LSDQA	L6I, Q9N, M94L, R98S, G114Q, Q178A	−
IN-Y-LSDQA	L6I, Q9N, M94L, R98S, G114Q, T117Y, Q178A	−
IY-Y-LSDQA	L6I, M10Y, M94L, R98S, G114Q, T117Y, Q178A	−
INY-LSDQA	L6I, Q9N, M10Y, M94L, R98S, G114Q, Q178A	−
INY-Y-LSDQA	L6I, Q9N, M10Y, M94L, R98S, G114Q, T117Y, Q178A	−
INL-LSDQA	L6I, Q9N, Q13L, M94L, R98S, G114Q, Q178A	−
INL-Y-LSDQA	L6I, Q9N, Q13L, M94L, R98S, G114Q, T117Y, Q178A	−
IYL-LSDQA	L6I, M10Y, Q13L, M94L, R98S, G114Q, Q178A	−
IYL-Y-LSDQA	L6I, M10Y, Q13L, M94L, R98S, G114Q, T117Y, Q178A	−
INYL-LSDQA	L6I, Q9N, M10Y, Q13L, M94L, R98S, G114Q, Q178A	−
INYL-Y-LSDQA	L6I, Q9N, M10Y, Q13L, M94L, R98S, G114Q, T117Y, Q178A	−
Q13L-LSDQ	Q13L, M94L, R98S, G114Q	−
Q13L-Y-LSDQ	Q13L, M94L, R98S, G114Q, T117Y	−
Q13L-LSDQA	Q13L, M94L, R98S, G114Q, Q178A	−
Q13L-Y-LSDQA	Q13L, M94L, R98S, G114Q, T117Y, Q178A	−

[a] MN4Rh-3 CA was constructed by replacing the CypA-binding loop and H6/7L of HIV-1_{NL4-3} CA with the corresponding regions of SIVmac239 CA and by the additional introduction of a Q110D mutation (Fig. 1) (19, 24).

[b] Amino acid number in MN4Rh-3 CA.

[c] Viral growth potential in M1.3S cells. ++++, grows similarly to MN4/LSDQ; +++, grows more efficiently than MN4Rh-3; ++, grows similarly to MN4Rh-3; +, grows more poorly than MN4Rh-3; −, undetectable during the observation period.

clones here, except for MN4Rh-3, exhibited a tendency to have a higher level of resistance to CyM-TRIM5α than to RhM-TRIM5α (Fig. 4). It has been shown that TRIM5α proteins encoded by *TRIM5*^{TFP} are more restrictive to virus infection than are those encoded by *TRIM5*^{Q} (40). The observed tendency for TRIM5α resistance may be due to the difference between RhM-TRIM5α (*TRIM5*^{TFP}) and CyM-TRIM5α (*TRIM5*^{Q}) used in the assay. These results indicate that the enhancement of viral growth in M1.3S cells by CA alterations depends, at least in part, on the increased resistance to TRIM5α.

Virus replication capability in macaque PBMCs with different *TRIM5* alleles reflects the TRIM5α resistance of HIV-1mt clones. We have previously shown that MN4Rh-3 replicates well in *TRIM5α/TRIM5CypA* heterozygous CyM PBMCs/individuals, but its replication was restricted in *TRIM5α* homozygous CyM PBMCs/individuals (19, 24). To confirm the effect of the increased resistance of MN4/LSDQ and MN5/LSDQ against macaque TRIM5α on viral replication, we examined their replication potential relative to that of MN4Rh-3 and MN5Rh-3 in *TRIM5α/TRIM5CypA* heterozygous or *TRIM5α* homozygous macaque PBMCs.

First, we compared viral growth potentials of the clones in CyM PBMCs (Fig. 5A). Growth kinetics of MN4Rh-3 and MN4/LSDQ were similar in *TRIM5α/TRIM5CypA* heterozygous CyM

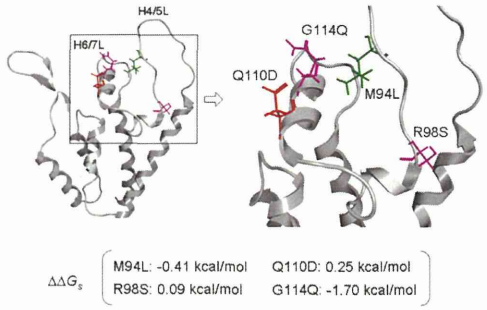

FIG 3 Structural analysis of the HIV-1mt CA NTD. A molecular model of the HIV-1mt CA NTD was constructed by homology modeling and refined as described previously (19). Single-point mutations were generated on the CA model, and ensembles of protein conformations were generated by using the LowMode MD module in MOE (Chemical Computing Group Inc., Quebec, Canada) to calculate average stability by using Boltzmann distribution. The stability scores ($\Delta\Delta G_s$) of the structures refined by energy minimization were obtained through the stability scoring function of the Protein Design application and are indicated below the structural model.

PBMCs. In contrast, the replication efficiency of MN4/LSDQ was markedly enhanced in *TRIM5*α homozygous CyM PBMCs relative to that of MN4Rh-3 (Fig. 5A). Similar results were obtained with RhM PBMCs. MN4Rh-3 exhibited growth kinetics comparable to those of MN4/LSDQ in *TRIM5*α/*TRIM5CypA* heterozygous RhM PBMCs (Fig. 5B). In *TRIM5*α homozygous RhM PBMCs, MN5/LSDQ replicated much more efficiently than MN5Rh-3 (Fig. 5C). CXCR4-tropic HIV-1mt clones (MN4 series) were found to exhibit a higher growth ability than CCR5-tropic HIV-1mt clones (MN5 series) in both M1.3S cells and macaque PBMCs (Fig. 2D and 5B and C) and were therefore used for experiments thereafter. In sum, the replication potential of TRIM5α-resistant HIV-1mt clones (MN4/LSDQ and MN5/LSDQ) markedly increased in *TRIM5*α homozygous PBMCs but was similar to that of TRIM5CypA-resistant/TRIM5α-sensitive clones (MN4Rh-3 and MN5Rh-3) in *TRIM5*α/*TRIM5CypA* heterozygous PBMCs. These results suggest that M94L/R98S/G114Q mutations in MN4Rh-3 CA largely contribute to the acquisition of TRIM5α resistance.

HIV-1 Vpu gains the ability to specifically counteract macaque tetherin by replacing its TM domain with the corresponding region of SIVgsn166 Vpu. Tetherin as well as TRIM5 proteins are important anti-HIV-1 factors in macaque cells (4, 8, 10), but the HIV-1mt clones constructed so far do not display macaque tetherin antagonism due to Vpu derived from HIV-1_{NL4-3}. It has been shown that Vpu from SIVmon/mus/gsn can antagonize macaque tetherin but not human tetherin (26). To confer the ability to counteract macaque tetherin on HIV-1mt clones, we modified the *vpu* gene. The sequence of the cytoplasmic domain of HIV-1 Vpu partially overlaps the 5′-end sequence of Env, and the TM domain of Vpu is a key region for species-specific tetherin antagonism (22). Thus, we constructed Vpu clones that contain SIVmon/mus/gsn TM and HIV-1mt cytoplasmic domains (Fig. 6A). First, RhM tetherin antagonism of various Vpu clones was analyzed by Vpu *trans*-complementation assays for virion release (Fig. 6B). 293T cells were cotransfected with a *vpu*-deficient HIV-1mt clone (MN4Rh-3-ΔU), an RhM tetherin expression vector (pCIneo-RhM tetherin), and various Vpu constructs, and virion production from cells on day 2 posttransfection was measured. While MN4Rh-3-ΔU released progeny virions efficiently upon transfection without RhM tetherin expression, its virion production was significantly inhibited in the presence of RhM tetherin. Although this reduction was not rescued by HIV-1_{NL4-3} Vpu, SIVmon/mus/gsn Vpu restored it to some extent, consistent with a previous report (26). Of the SIV/HIV-1 chimeric Vpu proteins, gsnTM-Vpu appeared to be somewhat better than the others and was therefore used thereafter.

Next, we examined the ability of HIV-1_{NL4-3} Vpu and gsnTM-Vpu to downregulate cell surface CD4 and tetherin (Fig. 6C). MAGI, LLC-MK2, and HEp2 cells were used for analysis of CD4,

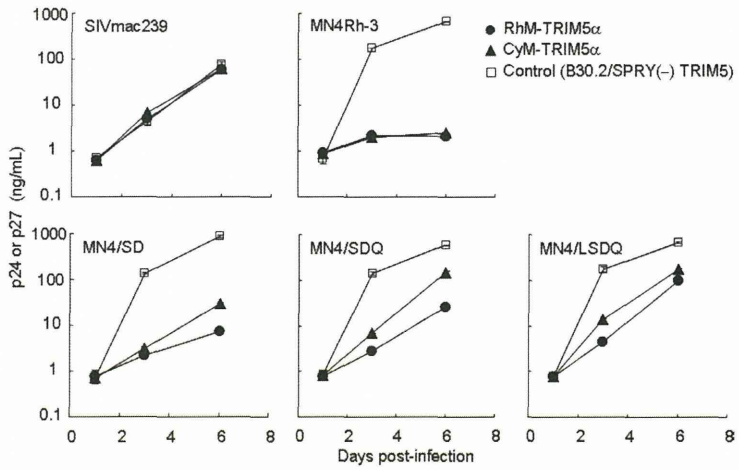

FIG 4 Susceptibility of SIVmac239 and various HIV-1mt clones to macaque TRIM5α. Human MT4 cells (10^5) were infected with recombinant SeV expressing RhM-TRIM5α (*TRIM5*^{RH}), CyM-TRIM5α (*TRIM5*^{CY}), or B30.2/SPRY(−) TRIM5. Nine hours after infection, cells were superinfected with 20 ng (Gag-p24) of various HIV-1mt clones or 20 ng (Gag-p27) of SIVmac239. Virus replication was monitored by the amount of Gag-p24 from HIV-1mt clones or Gag-p27 from SIVmac239 in the culture supernatants. Error bars show actual fluctuations between duplicate samples. Representative data from two independent experiments are shown.

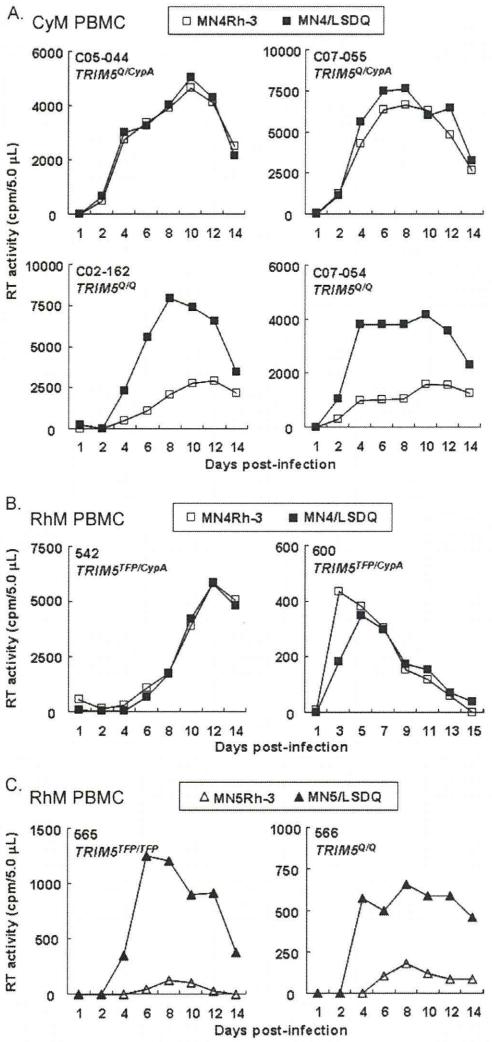

FIG 5 Growth kinetics of HIV-1mt clones with a distinct CA in macaque PBMCs. (A) Infection of PBMCs from four *TRIM5α*/*TRIM5CypA* heterozygous or *TRIM5α* homozygous CyM individuals. (B and C) Infection of PBMCs from four RhM individuals with different *TRIM5* alleles. For infection, input viruses were prepared from 293T cells transfected with the proviral clones indicated, and equal amounts (2.5×10^6 RT units) were used to spin infect PBMCs (2×10^6 cells). Virus replication was monitored by RT activity released into the culture supernatants. Monkey identification numbers are indicated in each panel.

RhM tetherin, and human tetherin, respectively. Cells were transfected with Vpu-green fluorescent protein (GFP) bicistronic expression plasmids and subjected to flow cytometry analysis on day 2 posttransfection. While both HIV-1_{NL4-3} Vpu and gsnTM-Vpu significantly decreased cell surface CD4 levels, the RhM tetherin level was reduced by gsnTM-Vpu but not by HIV-1_{NL4-3} Vpu. Similar results were obtained for MK.P3(F) cells expressing endogenous CyM tetherin (data not shown). In contrast, HIV-1_{NL4-3} Vpu but not gsnTM-Vpu downmodulated cell surface human tetherin. These results show that the transfer of the SIVgsn166 Vpu TM domain to HIV-1 Vpu is sufficient to confer the ability to specifically antagonize macaque tetherin on viruses.

gsnTM-Vpu in the context of proviral genome functions in macaque cells. To ask if gsnTM-Vpu is functional in the proviral context, we generated an HIV-1mt clone encoding gsnTM-Vpu (MN4/LSDQgtu) (Fig. 1 and 7A). Interestingly, it has been shown that Vpu of HIV-1 composed of HIV-1_{DH12} TM and HIV-1_{NL4-3} cytoplasmic domains counteracts macaque tetherin (22). We thus constructed another HIV-1mt clone, MN4/LSDQdtu, that has chimeric Vpu, as described above (Fig. 7A).

To examine the species-specific tetherin antagonism of these proviral clones, we carried out virion release assays in the presence of RhM or human tetherin (Fig. 7B). Using SIVmac239 Nef as a control antagonist against macaque tetherin (52, 53), the anti-macaque tetherin activities of MN4/LSDQ, MN4/LSDQdtu, and MN4/LSDQgtu were comparatively analyzed. As described above, SIVmac239 Nef exhibited the ability to specifically antagonize macaque tetherin. As expected, virion production of MN4/LSDQ and its *vpu*-deficient clone was similarly restricted in the presence of RhM tetherin, and MN4/LSDQ displayed a higher level of virion production than that of its *vpu*-deficient clone in the presence of human tetherin, indicating its specific antagonism to human tetherin. Also, as expected from a previous report (22), MN4/LSDQdtu showed both RhM and human tetherin antagonism, although its anti-RhM tetherin activity was relatively low. Strikingly, virion production levels of MN4/LSDQgtu in the presence of RhM/human tetherin were similar to those of SIVmac239. This indicates that MN4/LSDQgtu has specifically strong anti-RhM tetherin activity, as is the case for SIVmac239. To see if various Vpu proteins function during viral replication in macaque cells, we determined the growth properties of various HIV-1mt clones carrying distinct Vpu proteins. Although the effect of *vpu* deletion is virologically small, *vpu*-deficient viruses are readily distinguishable from the parental wild-type virus by comparative kinetic analysis of viral growth (22, 29). As shown in Fig. 7C, while MN4/LSDQ and MN4/LSDQdtu exhibited growth kinetics similar to those of their respective *vpu*-deficient clones, *vpu*-deficient MN4/LSDQgtu grew significantly more poorly than its parental virus. Taken together, it can be concluded that MN4/LSDQgtu Vpu but not MN4/LSDQ Vpu functions during viral replication in M1.3S cells. However, the functionality of MN4/LSDQdtu Vpu in macaque cells was not clear in the viral growth kinetics here. Although there are some possible explanations, the relatively low anti-RhM tetherin activity of MN4/LSDQdtu (see the results in Fig. 7B) could account for this observation.

Although the tertiary structure of the HIV-1 Vpu TM domain has been determined by NMR (38), the structure of the TM domain from SIV Vpu has not been solved to date. To investigate how replacement of the Vpu TM domain could lead to changes in TM structure, we constructed structural models of Vpu TM domains of MN4/LSDQ, MN4/LSDQdtu, and MN4/LSDQgtu (Fig. 7D). This modeling study revealed that the types of amino acid residues corresponding to the crucial residues (54) in HIV-1 Vpu for binding with human tetherin are similar between MN4/LSDQ and MN4/LSDQdtu, whereas they are often different in MN4/LSDQgtu. In addition, their steric locations in the helices are also similar between MN4/LSDQ and MN4/LSDQdtu, whereas they are very different in MN4/LSDQgtu. Finally, angles between the